Research Square

Preprints are preliminary reports that have not undergone peer review.
They should not be considered conclusive, used to inform clinical practice,
or referenced by the media as validated information.

Determination and Optimization of Nanofiber Morphologies for Delivery Potential According to the Steiner Minimal Trees

Caglar Sivri

caglar.sivri@bau.edu.tr

Bahçeşehir University

Research Article

Keywords: Steiner minimal trees, Nanofibers, Nanofiber networks Smart structures, Functional applications

Posted Date: June 29th, 2026

DOI: https://doi.org/10.21203/rs.3.rs-9939426/v1

License: This work is licensed under a Creative Commons Attribution 4.0 International License.
Read Full License

Additional Declarations: No competing interests reported.

Determination and Optimization of Nanofiber Morphologies for Delivery Potential According to the Steiner Minimal Trees

Çağlar Sivri [1]

[1] Faculty of Engineering and Natural Sciences, Department of Management Engineering, Bahçeşehir University, Istanbul 34349, Turkey; caglar.sivri@bau.edu.tr

Abstract

Drawing inspiration from nature offers possibilities not only for designing next-generation aircraft or high-speed trains on a macro scale, but also for designing nano-network structures or nanofiber structures for functional applications on a very small scale. This study involved experiments and analyses to determine the process conditions under which nanofiber structures, inspired by Steiner Minimal Trees found in nature, particularly in soap bubbles and/or spider webs, can be developed. Simultaneously, the similarities and differences between the obtained nanofiber structures and those found in previous studies were discussed, and theoretical inferences were made regarding their potential functional applications. Nanofibers obtained by applying two different polymers and process conditions were analyzed and colored using the Python language, and their Steiner Minimal Tree compatibility was tested. Accordingly, it was determined that the nanofibers most suitable for the Steiner Minimal Tree structure are those produced in polylactic acid polymer under specified conditions. Overall, these findings demonstrate that the Steiner Minimal Tree principles offer a useful biomimetic optimization framework for nanofiber design, reducing redundancy while preserving functionality.

Keywords: Steiner minimal trees, Nanofibers, Nanofiber networks Smart structures, Functional applications

1. Introduction

Repairing critical-sized bone defects and chronic skin wounds remains one of the major challenges in regenerative medicine [1,2]. In response, electrospun nanofibrous matrices have become important materials for these applications because they can act as scaffolds that mimic the extracellular matrix (ECM) while also serving as carriers for the localized delivery of bioactive proteins [3,4] . These scaffolds offer a highly porous structure and a very large surface-to-volume ratio, which helps support efficient mass transfer and improves the loading of therapeutic agents [3,5]. At the same time, nanofiber characteristics such as fiber diameter, alignment, and secondary porosity play a key role in influencing cell adhesion, cell proliferation, and nutrient transport [3,6]. In tissue engineering, one of the central strategies is to promote a coordinated response between angiogenesis and osteogenesis. This often depends on the sequential delivery of vascular endothelial growth factor (VEGF) and bone morphogenetic protein-2 (BMP-2) in order to reproduce the natural stages of healing [1,7]. In addition, regenerative membranes must provide strong barrier properties to block soft tissue invasion while still preserving an osteogenic microenvironment that supports bone formation [1,8]. The performance of these scaffolds depends heavily on how well drug release can be controlled across both space and time so that it matches the biochemical needs of the healing tissue [1,9]. Bioactive compounds obtained from sources such as Hypericum aqueous extracts or Centella asiatica have shown the ability to speed up recovery by regulating important signaling pathways, including the PI3K/Akt and TGF-β/Smad pathways [2]. To fully realize the delivery potential of these compounds, the internal structure of the nanofiber matrix needs to be

topologically optimized so that transport distances are reduced without compromising mechanical strength [10,11]. Advanced computational approaches, together with Steiner tree principles, provide a useful basis for designing such highly efficient networks [10,12]. By incorporating optimized path lengths into the porous architecture, the matrix can achieve better delivery performance and distribute therapeutic agents more effectively, which may help support synchronized tissue regeneration [1].

The Steiner Minimal Tree (SMT) problem offers a mathematical basis for identifying the shortest possible network that connects a given set of terminal points [13,14]. SMT is a classical NP-hard combinatorial problem and has important applications in areas such as chip design, network routing, and computational biology [10]. Nature also provides biologically inspired examples of solutions to this problem, including the minimum-energy configurations formed by bubble surface tension and the exploratory behavior of the slime mold Physarum polycephalum [11]. The same principles are relevant for the efficient routing of pipelines and cables in complex engineering systems [10]. In addition, the use of Steiner tree structures has shown promise for improving both mechanical stability and path efficiency in nanotechnology and advanced textile engineering [11,12] In drug delivery, identifying the most efficient network morphology is especially important for maximizing the transport of bioactive substances through porous matrices. For this reason, the present study seeks to determine and optimize nanofiber morphologies based on Steiner Minimal Trees in order to improve their structural efficiency and delivery potential in regenerative medicine, energy storage and other various functional applications.

2. Materials and Methods

In this work, polymeric solutions were used to produce nanofibers via electrospinning method. Python language has been used to analyze the images for their compatibility to the Steiner Minimal Trees.

2.1. Materials

2 different polymers were used for nanofiber production. Polyvinyl alcohol (PVA) polymer has been purchased from Sigma Aldrich Company and utilised as supplied. Polylactic Acid (PLA) polymer supplied by NatureWorks LLC has been used as received. A total of 3.48 g of PVA polymer was mixed with 17 mL of distilled water and stirred mechanically at 80°C for six hours until it dissolved completely. As a result, about 20.5 mL of an aqueous PVA solution with a concentration of 17 wt% was obtained. A total of 8 g of PLA polymer was combined with 24 mL of distilled water and mechanically stirred at 80°C for eight hours until it was fully dissolved. This produced an aqueous PLA solution with a concentration of 25 wt%.

2.2. Methods

Electrospinning was used for fabrication of nanofibers with different morphologies while python language has been used for image analysis. Scanning Electron Microscopy (SEM) analysis was used for morphology investigation. Details of the methods have been provided in more detail at following subsections.

2.2.1. Electrospinning

Electrospinning was carried out using simple-to-prepare solutions of PVA and PLA polymers and a conventional setup consisting of an electronic syringe pump, a syringe, a high-voltage power supply, and a collector plate (Figure 1). This study used an electrospinning device made by Inovenso Ltd. & Inc., a Turkey-based company. Different process conditions were applied for these two different solutions.

Nanofibers from PVA solution were produced at 14 kV voltage, 10 cm of collector plate to needle tip distance, 2 mL/h feeding rate and 10 minutes duration. Nanofibers from PLA

solution were produced at 25 kV voltage, 10 cm of collector plate to needle tip distance, 3 mL/h feeding rate and 10 minutes duration. The resulting fibers were dried under vacuum at 50 °C for 24 hours. In addition to the two different nanofibers produced within the scope of this study, Steiner minimal tree analysis was also performed on two different nanofibers obtained from previous studies for reference and comparison purposes.

2.2.2. SEM Characterization

The morphology and orientation of the nanofibers were examined using a scanning electron microscope (LEO 440; Technical Sales Solutions, Beaverton, OR, USA).

2.2.3. Image Analysis via Python

Microscopy images of the nanofibers were processed in Python through a custom workflow designed to measure morphological features linked to connectivity and delivery potential. The images first underwent grayscale conversion, contrast adjustment, and noise filtering, followed by binarization and skeletonization to retain the overall topology of the fiber network. Key structural features, including endpoints, branch points, and intersections, were then identified and used to build graph-based representations of the nanofiber architecture. Steiner Minimal Tree analysis was applied to determine near-optimal connection paths between the selected nodes. Based on these networks, metrics such as total connection length and branching behavior were calculated to compare differences in nanofiber morphology. Overall, this Python-based method offered a reproducible and objective way to evaluate structural characteristics associated with Steiner minimal tree architectures. The images have been produced in two types: (**a**) Steiner compatibility overlay (**b**) Cycle-free backbone (bridges only).

Legends that are seen on the Python produced images for Steiner compatibility overlay explained as follows;

Green = bridge / tree-like segment (cycle-free; compatible with a Steiner tree idea)

Red = cycle edge (cannot be part of a Steiner minimal tree, because SMTs have no cycles)

Orange = mixed pixels touching both bridge + cycle regions

Blue dots = endpoints

Magenta dots = high-degree junctions (deg ≥ 4), which are atypical for clean Steiner junction structure

Also included is a second view that displays only the cycle-free backbone (bridges only)—that is, the portion that could serve as an SMT-like "skeleton" if terminals are defined later.

3. Results

In this part, compatibility of nanofiber morphologies to Steiner minimal tree architectures (SMTA) was assessed using SEM images analyzed with Python. 4 different SEM images were taken as basis and then the images have been colored to show SMT compatibilities. The first 2 SEM images were selected from the previous studies of the author to serve as a reference with the comparison aim. The other two SEM images have been produced within the study using electrospun nanofibers.

Figure 2 illustrates nanofibers produced from gelatin polymer (NGEL) of 10 wt% and olive oil addition at 18 kV applied voltage with a gelatin feeding rate of 1.9 ml/h and olive oil feeding rate of 0.2 ml/h and 8 cm needle-tip to collector distance.

Figure 3. shows compatibility of the nanofiber morphologies produced from gelatin polymer and olive oil addition to SMT architectures. Most parts of the structure here form loops, shown in red - around 78 percent. 17% are bridge-only (green). A small share, four percent, acts both ways, marked orange. That mix explains why matching ideal branching patterns stay poor in terms of compatibility with SMTAs until pulling out a simplified network comes first.

Figure 4 illustrates nanofibers produced from PEO polymer (NPEO) of 16 wt% at 17 kV applied voltage with a feeding rate of 5 ml/h and 10 cm needle-tip to collector distance and 1 hour duration. A distance positioning apparatus was used allowing polymer to be fed from different points in order to produce nanofibers in variable morphologies.

Figure 5. shows SMT architecture compatibility of the nanofiber morphologies produced with distance positioning apparatus from PEO polymer. For this image, compatibility with a Steiner minimal tree is limited: only about 11.9% of the skeleton edges are bridge-like, whereas 88.1% belong to cycles. Most of the skeleton forms loops - just under twelve percent act like bridges. This setup leans heavily on interconnected cells instead of sparse links. Loops take over here, not branching connections. One way to look at it: the picture shows every node linked directly, yet full of cycles - that stops it being a true Steiner minimal tree, since those never have loops. Even if three-line crossings pop up often, mimicking parts of Steiner patterns, the whole shape leans more toward something thick, like bubbles packed tight. From here, someone might pull out a cleaner branching frame, trimming down into a tree version later.

Figure 6 illustrates nanofibers produced from PVA polymer (NPVA) of 17 wt% at 14 kV voltage, 10 cm of collector plate to needle tip distance, 2 mL/h feeding rate and 10 minutes duration.

Figure 7. shows SMT architecture compatibility of the nanofiber morphologies produced from PVA polymer. The image is mostly red, suggesting that the projected network is far more looped and redundant than tree-like. Based on the 2D skeleton approximation I used, about 15.7% of the edges behave like bridges or tree edges, whereas roughly 84.3% contribute to forming cycles, resulting in an estimated 14,104 independent cycles in the projected network. The arrangement has very little resemblance to a Steiner minimal tree, with an approximate score of 2–3/10. The proper comparison will need to identify the end points of the network, but based on just its structure, it cannot be said to resemble a Steiner minimal tree even when accounting for the fact that this particular image is only a two-dimensional SEM projection of the three-dimensional network of fibers, wherein some of the apparent cross-overs might not actually represent physical cross-links.

Figure 8 illustrates nanofibers produced from PLA polymer (NPLA) of 25 wt% at 25 kV voltage, 10 cm of collector plate to needle tip distance, 3 mL/h feeding rate and 10 minutes duration.

Figure 9. shows SMT architecture compatibility of the nanofiber morphologies produced from PLA polymer. In this case, the compatibility between the current pattern and a Steiner minimal tree is expected to be low to moderate. According to the image, the skeleton consists of about 35.2% of bridges and 64.8% of cycles, with approximately 768 cycles in the 2-dimensional projection network. In the same way, the overall pattern based on the SEM network is also considered very compatible (about 2/10), since only about 14% of the estimated 3,706 edges have tree-like behavior (acting as bridges), whereas the remaining 86% act as redundant connections, forming about 1,100 cycles.

4. Discussion

The manuscript examines the nanofiber morphologies for their compatibilities to SMTAs and whether this compatibility could be used for a potential and theoretical prediction of the utilization of the nanofibers in delivering substances.

Graph-based analysis of the four nanofiber morphologies showed that every sample formed a globally connected network, but none perfectly met the core criterion of a Steiner minimal tree (SMT): a loop-free minimal network spanning a defined set of terminal points. Instead, all of the images were characterized by closed loops, redundant connections, and junction arrangements that only low to moderate matched Steiner-like branching. As a result, these morphologies are better understood as SMT-inspired transport networks rather than exact SMT configurations. Even though

not sounding as perfect, this inspiration might bring effectiveness and easy scalability as it was stated in different areas within the literature [17,18] .

NGEL exhibited a dense planar cellular structure containing roughly 2000 independent cycles. Although about 75% of the simplified junctions were three-way nodes, which is locally consistent with Steiner-type branching, only around 17% of the skeleton consisted of bridge-only segments, while nearly 78% was linked to cyclic regions. This suggests that the morphology preserved local geometric traits associated with efficient branching, but lost global SMT consistency because of extensive loop formation. Therefore, NGEL is more appropriately described as a redundant cellular network from which an SMT-like backbone might be derived, rather than as an inherently minimal topology [19].

A comparable pattern was found in NPEO. The projected network remained a single connected component with 31,641 skeleton nodes and 31,992 edges, corresponding to about 352 independent cycles. Only about 11.9–13.3% of the edges functioned as bridges, whereas 86.7–88.1% participated in cyclic connectivity. Junction analysis also revealed that degree-3 nodes were dominant (n = 578), while the number of endpoints was very small (n = 50), which does not perfectly align with a tree-like network. Therefore, even though local Steiner-like branching was present, NPEO was structurally far closer to a loop-rich cellular web than to a genuinely minimal connecting network [20].

NPVA showed the lowest overall alignment with SMT topology. Depending on the level of graph simplification, only about 12.4–15.7% of the segments acted as bridge-like elements, while 84.3–87.6% contributed to cycle formation, with roughly 11,436–14,104 independent cycles. This made it the most redundant and highly entangled projected network among all of the images analyzed. In contrast, NPLA, although still clearly non-Steiner on a global scale, preserved a somewhat higher bridge-rich portion after overlay analysis, with about 35.2% bridge-like compared with 64.8% cycle-like skeleton. Even so, the simplified projection still showed substantial redundancy, containing around 768–1100 cycles. On that basis, NPLA appears to provide the closest balance between network continuity and partial tree-like organization [21].

Overall, these findings indicate that the dominant structural pattern across all images was not minimal connection, but redundant area coverage. This distinction is important. From a mathematical standpoint, SMT optimization minimizes total path length and eliminates cycles [22] . In the nanofiber morphologies studied here, however, frequent three-way branching existed alongside widespread loop formation, which means that locally Steiner-like geometry did not produce global minimality [23]. Another limitation is that compatibility was assessed using 2D SEM projections without a predefined terminal set. Some apparent crossings may therefore reflect overlapping fibers rather than true fused junctions, and the reported cycle counts should be viewed as comparative topological descriptors rather than exact 3D graph invariants.

As for the working hypothesis concerning the expected correlation of increased SMT compatibility with superior delivery performance, its support was only partial. Strictly speaking, an optimal SMT is a desirable morphology when the goal is to interconnect distinct terminal sites using the shortest total path distance and the least amount of material. However, drug-delivery or other substance-delivery structures for bone remodeling and wound healing must, among other things, cover a broad surface area, contain local reservoir capacity, and have multiple release sites – properties not strictly relevant to a SMT, in addition to the requirement for local resilience against transport failure [24,25] .

With that said, the mismatch between the observed network morphology and that of the strict SMT cannot simply be considered a drawback. NGEL and NPEO are examples of networks with very dense structure and almost no bridges; as such, they may represent coverage-oriented rather than path-length oriented structures. As already stated, extensive coverage of the surface by exposed drug-containing fibers provides certain advantages in depot-type local delivery scenarios requiring rapid wetting and access to numerous release interfaces, especially for topical or implant-assisted applications necessitating contact across the defect bed area [26]. In short, while these

networks are far from being efficient in the strictest sense of the term SMT, they can still prove efficient in terms of area-wide release [27].

In turn, NPVA appears to be the ultimate case of such a behavior pattern. The extremely high cycle burden implies that the given morphology will contain high redundancy and large interfacing surface area, properties favorable to local loading and release capabilities but detrimental to shortest-path transport efficiency [28]. Hence, the concept of minimum energy and minimum time applies to this structure in analogy rather than literally. In other words, minimum energy and minimum time are to be taken here in the sense of minimum transport resistance and minimal transport route length, respectively, and not as biochemical energy. In this case, while NPVA is unlikely to act as a minimum network in the SMT context, it could still be efficient as such in terms of local release functionality [29].

Finally, NPLA strikes a good balance between both requirements, featuring an intermediary number of bridges that should allow for retaining some direct connection while allowing area-wide interface distribution [30]. In sum, one can conclude that the present study shows the most beneficial SMT-inspired design target for nanofiber drug delivery is neither a perfect tree nor one with excessive redundancy, but an intermediate structure with low but non-zero bridging ratio [31].

These findings also show that morphology on its own is not enough to define delivery performance. SEM-based topological analysis can support a structural explanation for loading potential and transport behavior, but it cannot by itself confirm high encapsulation efficiency, sustained release, or biological activity. Those outcomes still depend on factors such as polymer chemistry, fiber diameter distribution, pore architecture, hydrophilicity, degradation kinetics, and where the cargo is located within or on the fiber [32]. Therefore, the present results should be understood as highlighting morphologies with promising delivery potential rather than proving actual delivery efficacy [33].

As they currently appear, the dense and highly exposed fiber surfaces, particularly in images of NGEL, NPEO, NPVA would probably encourage a rapid initial release if therapeutic agents were added through simple blend electrospinning or surface adsorption. This kind of response could be useful in applications that benefit from an early antimicrobial or anti-inflammatory burst [34]. However, it would be less appropriate for the prolonged and staged release needed to support synchronized regenerative signaling in bone and skin repair. For this reason, the loop-rich morphologies identified in this study would be better used alongside cargo-protective approaches such as core-shell fibers, nanoparticle-in-fiber encapsulation, multilayer structures, or crosslinked barrier domains [35]. In those cases, the same large interfacial area that promotes rapid wetting could be preserved while diffusion from the internal reservoir is more effectively controlled.

Another major implication of this study is the idea that regenerative drug delivery is best served by a hybrid rather than a purely Steiner topology [36]. While the former may reduce the length of the system, it could sacrifice other factors such as surface area, release-site density, and spatial buffer. On the other hand, a loop-rich scaffold can create excellent reservoir and release behavior but fail to achieve transport minimality [37]. The ideal design for drug delivery would thus incorporate the principles of SMT into an overall framework of connected bridges and looped nanofibers. For example, the backbone of such a design would optimize the long-distance transport while the loops would function as local reservoirs and release regions. Such a design can prove particularly valuable in guided bone regeneration and chronic wound dressings, which require a combination of spatial distribution and temporal control over delivery [38].

NPLA is clearly the best option among the four morphologies under analysis in terms of its suitability for designing optimal hybrid scaffold structures because it retained the highest fraction of usable bridges without sacrificing connectivity required for area-wide delivery [39]. NPVA, on the other hand, appears more appropriate when designing a product that requires greater reservoir capacity and localized release capability rather than directed transport [40]. Finally, NGEL and NPEO fall into the middle ground, combining high level of connectivity with minimal global minimality. The future steps to take in optimizing the selected scaffold will thus involve identifying

biologically relevant endpoints – defects, vascular entries, and other relevant areas – and applying selective pruning of the scaffold structure.

As previously stated in different terms, simple geometric arrangements are necessary to create a Steiner minimal tree structure; for example, the angle between two adjacent branches must be 120° and all three branches must have equal radii.

Nano-networks with soap bubble/spider web/honeycomb appearance tend to conform to the Steiner tree model; when jets or droplets undergo phase separation along the Steiner geometry, they enter an optimization phase separation mode, with the least amount of material and the most void droplets inevitably attracting for phase separation [42]. The lowest energy principle enables the formation of nano-networks; nano-networks tend to complete phase separations with the lowest energy [43].

When all of the SMT inspired nanofibers morphologies from the literature or newly developed ones within the study have been considered, the most common features could be listed as extremely small diameter, high porosity, Steiner tree network geometry. While previous studies have mentioned that these structures could be used in areas such as filtering harmful nanoparticles or preventing viruses, there has been no mention of their potential for drug delivery or transporting other materials.

Finally, considering the current literature I have encountered in this field, it is believed that the structure shown in Figure 10 best meets the criteria discussed in this article among structures produced from nanofibers and exhibiting STM morphology. However, the extent to which the structure in the aforementioned figure meets the criteria such as "a tree: connected or acyclic; Steiner point (an added junction) must be a degree-3 node; if all triangle angles are less than 120; being noncrossing; having degree-3 Steiner points; bottleneck bounds for longer Steiner paths; lunar region sharpening; and the clover-region restriction" has not been examined in detail, and new studies can be conducted taking all these criteria into account.

In summary, the nanofiber morphologies under analysis have demonstrated very limited compliance with the principles of SMT but significant potential as scaffolds for local drug delivery. The key asset here is not necessarily minimized global transport but rather the combination of interconnectedness, substantial surface area, and many release sites. In other words, from the perspective of current biomimetic models, SMT should be seen more as a guiding principle than a desired morphology per se.

5. Conclusions

The nanofiber morphologies in this study were examined using the concept of Steiner Minimal Trees to evaluate how suitable they might be for functional applications such as drug or substance carrying, regenerative medicine scaffolds, energy storage and etc. The findings revealed that, although all of the nanofiber networks were fully connected overall, none perfectly matched the acyclic and strictly minimal structure of a true Steiner tree. Instead, the networks were mainly rich in loops and showed clear topological redundancy, suggesting that their organization is influenced more by the need for spatial coverage and interfacial continuity than by simple path minimization.

This indicates that a pure Steiner topology is not necessarily the best standalone design goal for therapeutic nanofiber systems. While Steiner-like networks can be beneficial for shortening transport pathways, regenerative scaffolds also need to ensure broad contact with tissue, multiple release points, local storage capacity, and structural resilience. For that reason, the most effective design is likely to be a hybrid architecture, one that combines an SMT-inspired backbone for efficient connectivity with carefully controlled cyclic regions that support distributed release and functional stability.

Among the samples analyzed, the NPLA morphology appeared to be the closest to an SMT-inspired arrangement because it preserved the highest proportion of bridge-like connections while still maintaining overall network continuity. This makes it the most promising candidate for balancing transport efficiency with delivery performance. On the other hand, the morphologies with

stronger loop dominance may be better suited to applications where widespread local release is more important than direct shortest-path transport.

Overall, these findings show that Steiner Minimal Tree principles can serve as a useful biomimetic strategy for optimizing nanofiber design, not as a strict final topology, but as a mathematical framework for reducing unnecessary redundancy while still maintaining the multiple functional demands of regenerative delivery systems. Future work should combine 3D structural analysis with experimental studies of drug loading, release behavior, diffusion, and cellular response in order to develop topology-based design rules for advanced nanofibrous scaffolds used in bone repair and wound healing.

Funding: This research received no external funding.

Institutional Review Board Statement: Not applicable.

Informed Consent Statement: Not applicable.

Data Availability Statement: The original contributions presented in this study are included in the article/supplementary material. Further inquiries can be directed to the corresponding author(s).

Acknowledgments: I would like to express my sincere gratitude to the KTH Royal Institute of Technology in Sweden's 'Biomimetic Fiber Engineering' program, which contributed to the formation of the vision behind this study, and to the courses and laboratory work I undertook within the program, such as Biomime Subjects, Biofiber Resources, Wood Biology, and Polymer and Fiber Science, as well as to Prof. Dr. Henrik ASPEBORG, who served as the director of this program.

Conflicts of Interest: The authors declare no conflicts of interest.

References

1. X. Chen, T. Zhang, H. Li, Y. Chen, B. Zhang, Y. Wang, W. Zhang, R. Zhang, Y. Wang, Q. Zhou, W. Lu, Y. Guo, and J. Wu, Mater. Futures **5**, 015401 (2026).
2. Q.-Q. Xiong, M.-J. Chen, S. Cheng, J. Yu, M. Ahmad, and H. Luo, Food & Medicine Homology (2025).
3. X. Dai, W. Nie, H. Shen, H.-G. Machens, K. Böker, S. Taheri, W. Lehmann, Y. Shen, and A. F. Schilling, Regenerative Biomaterials **12**, rbae139 (2025).
4. A. Muscolo, O. Mariateresa, T. Giulio, and R. Mariateresa, IJMS **25**, 3264 (2024).
5. K. Shahane, M. Kshirsagar, S. Tambe, D. Jain, S. Rout, M. K. M. Ferreira, S. Mali, P. Amin, P. P. Srivastav, J. Cruz, and R. R. Lima, Pharmaceuticals **16**, 611 (2023).
6. E. H. D. Siregar, J. W. Gunadi, and T. L. Wargasetia, NRFHH **5**, 330 (2025).
7. Z. Cheng, Z. Cui, Z. Li, S. Galmarini, Y. Liu, H. Wang, H. Kui, Y. Zhou, C. Morton, S. Li, G. Zeng, Z. Xiong, M. Fu, Y. Li, R. Zboray, Y. Yang, R. Zhou, R. Yu, J. Shen, S. Lu, C.-Y. Yang, S. Zhao, L. Zhao, and H. Wu, Nat Sustain **8**, 957 (2025).
8. V. Blanco, G. González, and J. Puerto, Computers & Industrial Engineering **207**, 111331 (2025).
9. Z.-X. Yang, X.-Y. Jia, J.-Y. Hao, and Y.-P. Gao, Journal of Applied Mathematics **2013**, 1 (2013).
10. A. Sadeghi and H. Fröhlich, BMC Bioinformatics **14**, 144 (2013).
11. S. Hsu, F. I. S. Massolo, and L. P. Schaposnik, Sci Rep **12**, 14536 (2022).
12. M. Brazil, R. L. Graham, D. A. Thomas, and M. Zachariasen, Arch. Hist. Exact Sci. **68**, 327 (2014).
13. D. Chen, D.-Z. Du, X.-D. Hu, G.-H. Lin, L. Wang, and G. Xue, Theoretical Computer Science **262**, 83 (2001).
14. D. Bilò, Algorithmica **86**, 2652 (2024).
15. Ç. Sivri, K. Aksoy, and S. Demirbağ, Natural Sciences and Technology 103 (2013).
16. Ç. Sivri, (2014).
17. Z. Li, X. Zhang, Z. Tan, C. Peng, X. Wu, and M. Zhu, Electronics **14**, 3931 (2025).
18. T. Polzin, (2003).
19. M. Molnár and B. M. Hassan, Algorithms **19**, 232 (2026).

20. A. Farrokhabadi, H. Lu, A. Sreekumar, M. M. Ashrafian, and D. Chronopoulos, Thin-Walled Structures **219**, 114238 (2026).
21. G. Liu, L. Yang, S. Xu, Z. Li, Y.-C. Chen, and C.-H. Chen, PeerJ Computer Science **7**, e473 (2021).
22. D. F. Abd, H. M. Sidqi, and O. H. Ahmed, Computers **14**, 422 (2025).
23. R. L. Church, Z. Drezner, F. Plastria, and A. Tamir, Computers & Operations Research **173**, 106825 (2025).
24. P. Trucillo, Materials **17**, 456 (2024).
25. S. Paramshetti, M. Angolkar, A. Al Fatease, S. M. Alshahrani, U. Hani, A. Garg, G. Ravi, and R. A. M. Osmani, Pharmaceutics **15**, 1204 (2023).
26. B. K. Dejene, M. A. Abtew, and B. G. Worku, Materials Today Advances **28**, 100655 (2025).
27. X. Duan, H. Chen, and C. Guo, J Mater Sci: Mater Med **33**, 78 (2022).
28. L. Blagojevic and N. Kamaly, Nano Today **61**, 102645 (2025).
29. D. Alves, J. C. Araújo, R. Fangueiro, and D. P. Ferreira, Molecules **28**, 3053 (2023).
30. I. Jarak, I. Silva, C. Domingues, A. I. Santos, F. Veiga, and A. Figueiras, IJMS **23**, 8581 (2022).
31. M. Alfadhel, CDD **23**, 44 (2026).
32. S. Y. Tan, N. S. Shahril Effendy, N. F. Ramli, N. Mohd Thani, S. J. Lim, W. A. Wan Mustapha, A. Azmi, and S. M. Mustapa Kamal, Trends in Food Science & Technology **167**, 105424 (2026).
33. Y. Tomar, N. Pandit, S. Priya, and G. Singhvi, ACS Omega **8**, 18340 (2023).
34. S. Jose M and S. Sumathi, Journal of Science: Advanced Materials and Devices **10**, 100933 (2025).
35. X. Lu, C. Shen, Z. Zhang, E. Barrios, and L. Zhai, ACS Appl. Mater. Interfaces **10**, 4041 (2018).
36. B. Okmen Altas, G. D. Kalaycioglu, S. Lifshiz-Simon, Y. Talmon, and N. Aydogan, Mol. Pharmaceutics **21**, 633 (2024).
37. N. Desai, H. E. Colley, Y. Krishna, L. A. Bosworth, and V. R. Kearns, Drug Deliv. and Transl. Res. **16**, 1096 (2026).
38. J. Lim, K.-J. Jang, H. Son, S. Park, J. Kim, H. Kim, H. Seonwoo, Y.-H. Choung, M. Lee, and J. Chung, Polymers **13**, 60 (2020).
39. A. Rahman, K. F. Tanvir, H. K. Jui, Md. T. Ahmed, S. M. A. Nipu, and S. B. Hussain, Results in Engineering **27**, 106156 (2025).
40. G. C. Türkoğlu, N. Khomarloo, E. Mohsenzadeh, D. N. Gospodinova, M. Neznakomova, and F. Salaün, IJMS **25**, 1668 (2024).
41. Y. Yin, Y. Chen, J. Yin, and K. Huang, Nanotechnology **17**, 4941 (2006).
42. G. Li, Y. Yin, Y. Li, and Z. Zhong, Chin. Sci. Bull. **54**, 3220 (2009).
43. X. Wang, B. Ding, G. Sun, M. Wang, and J. Yu, Progress in Materials Science **58**, 1173 (2013).

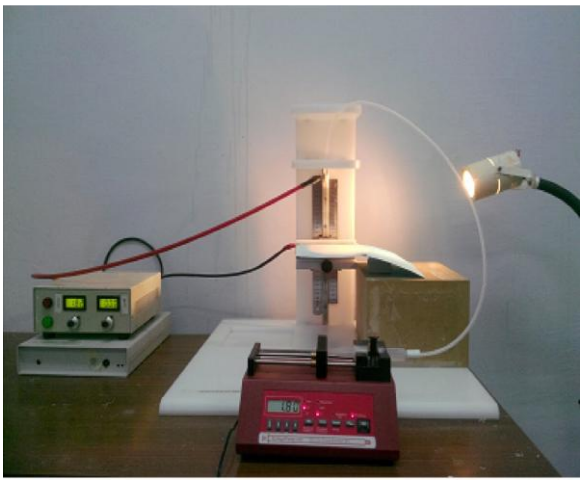


Figure 1. Electrospinning setup.

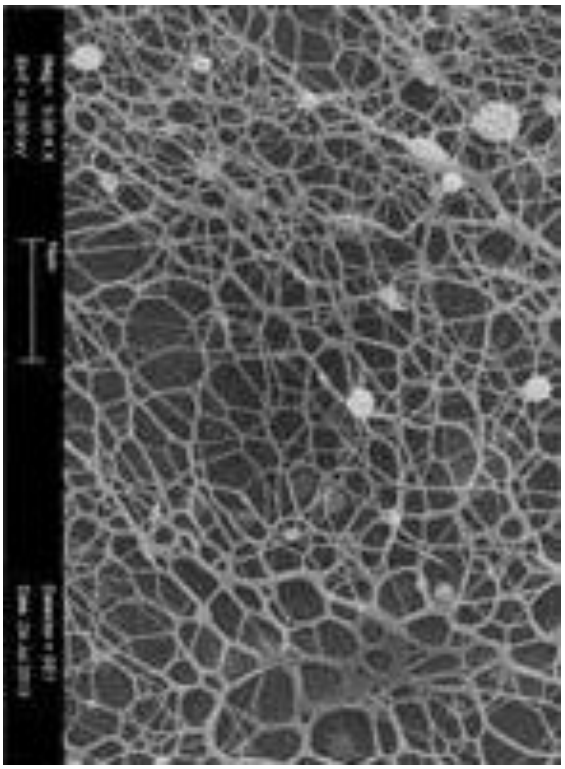
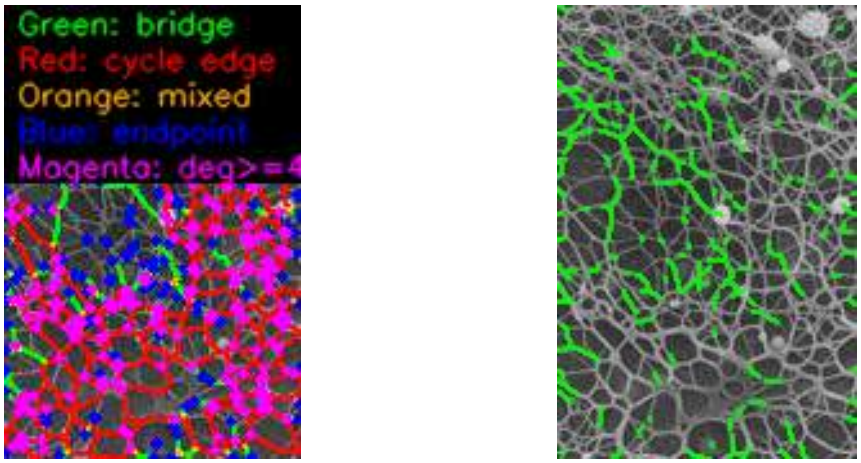


Figure 2. SEM images of nanofibers from Gelatin and Olive Oil [15]



(**a**) (**b**)

Figure 3. Compatibility analysis using SEM images of nanofibers from Gelatin and Olive Oil (**a**) Steiner compatibility overlay (**b**) Cycle-free backbone (bridges only).

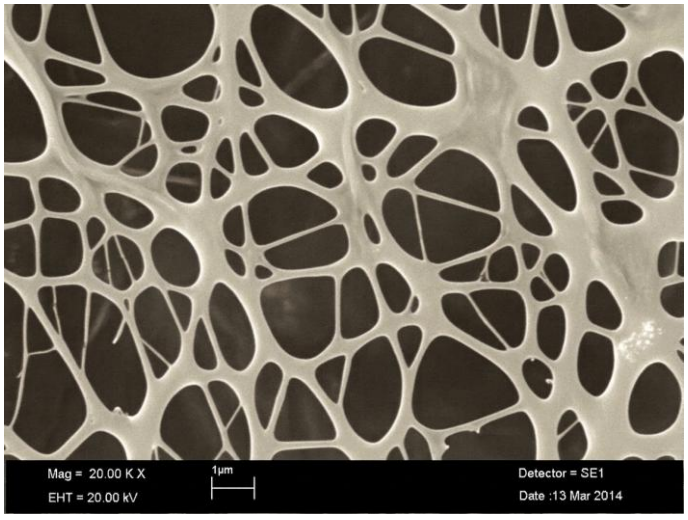
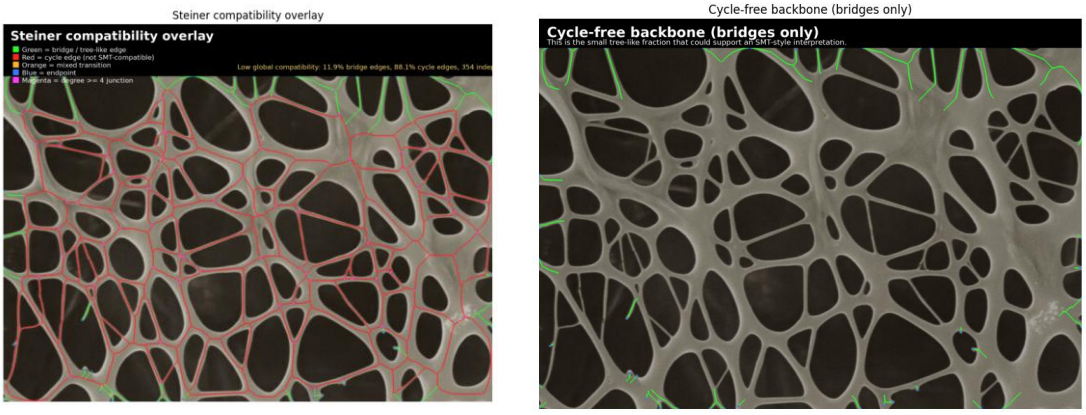


Figure 4. SEM images of nanofibers produced with distance positioning apparatus from PEO polymer [16]



(**a**) (**b**)

Figure 5. Compatibility analysis using SEM images of nanofibers produced with distance positioning apparatus from PEO polymer (**a**) Steiner compatibility overlay (**b**) Cycle-free backbone (bridges only).

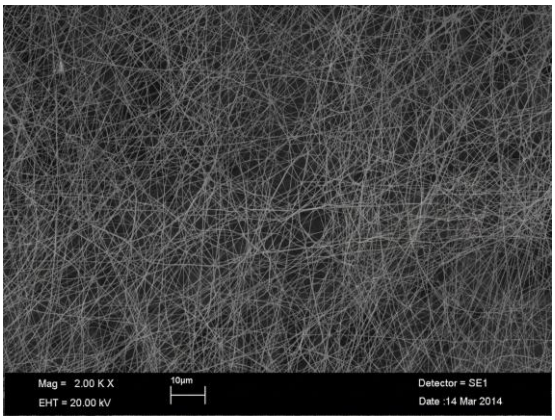
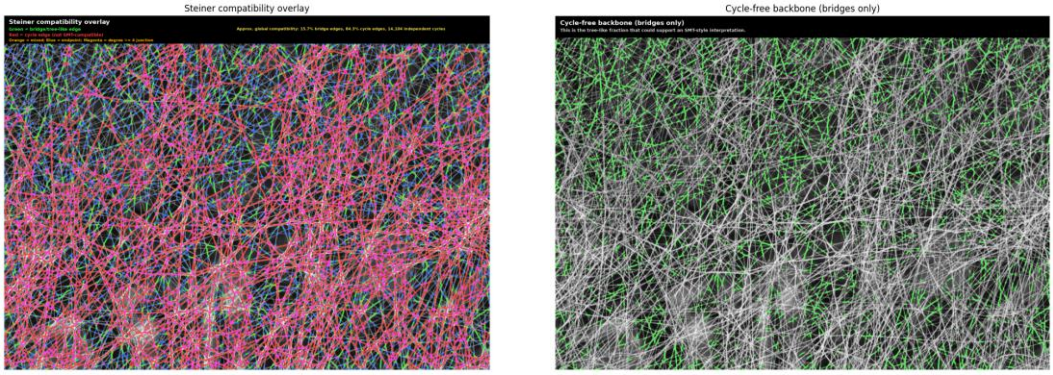


Figure 6. SEM images of nanofibers produced from PVA polymer



(**a**) (**b**)

Figure 7. Compatibility analysis using SEM images of nanofibers produced PVA polymer (**a**) Steiner compatibility overlay (**b**) Cycle-free backbone (bridges only).

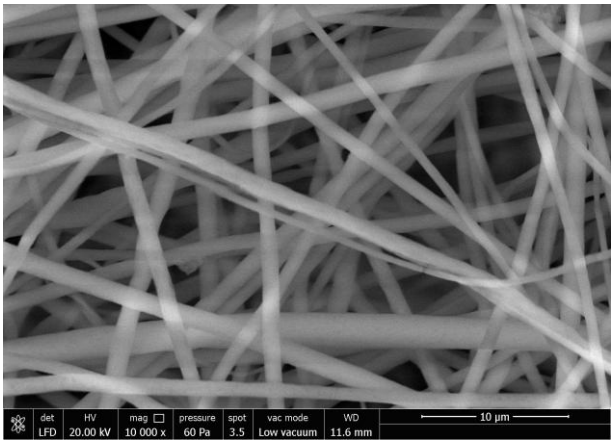
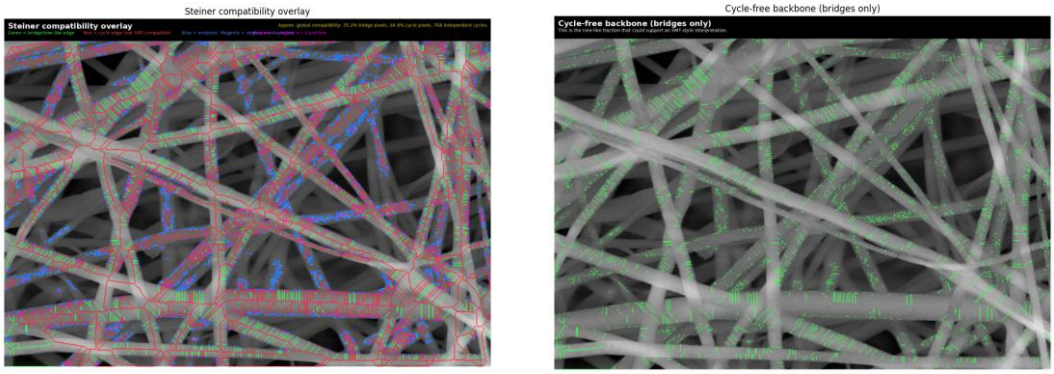


Figure 8. SEM images of nanofibers produced from PLA polymer



(**a**) (**b**)

Figure 9. Compatibility analysis using SEM images of nanofibers produced PLA polymer (**a**) Steiner compatibility overlay (**b**) Cycle-free backbone (bridges only).

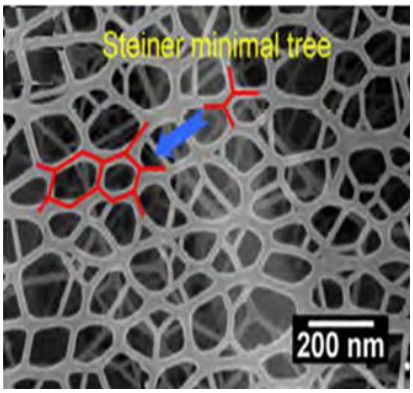


Figure 10. Configuration of a nanochannel template and fibers with a nanonetwork structure built with nanochannels having symmetric Y-shaped branches according to the Steiner minimal tree model [41]